ORIGINAL ARTICLE

Determination of the optimal milling feed direction for unidirectional CFRPs using a predictive cutting-force model

Dong-Gyu Kim[1,2] · Yun-Chul Jung[1] · Sung-Hwan Kweon[2] · Seung-Han Yang[2]

Abstract

To minimize the cutting force during milling of unidirectional carbon-fiber-reinforced plastics (CFRPs), we present a method that uses a predictive cutting-force model to optimize the feed direction. A CFRP with six different absolute fiber-orientation angles was used to derive specific cutting forces. Cutting force was predicted using regression of the specific cutting force and verified by milling tests, with 2–10-mm radial depths of cut at each fiber-orientation angle. The fiber cutting angle, which significantly affects CFRP cutting characteristics, can easily be changed by varying the feed direction. Therefore, the optimal feed direction is derived by predicting the cutting force in the feed direction in the range 0–180° using the cutting-force model and comparing the cutting forces in all feed directions. The optimal feed direction is expressed by a second-order polynomial function of the radial depth of cut. In the validation of the proposed method, the cutting force and cycle time in the optimal feed direction were reduced by 54% and 53%, respectively. Because only the feed-direction angle is changed, which is a relatively easy adjustment in the milling process, this method efficiently reduces the cutting force in CFRP milling. Also, as a predictive cutting-force model is employed, it is possible to derive the optimal feed direction under various cutting conditions with minimal experimentation.

Keywords CFRP · Milling · Cutting-force model · Feed direction · Fiber cutting angle

Nomenclature

$\varnothing$	Fiber cutting angle (deg)
θ	Cutting-tool rotation angle (deg)
θ_S	Cutting-tool entry angle (deg)
R_d	Radial depth of cut (mm)
D	Cutting-tool diameter (mm)
θ_E	Cutting-tool exit angle (deg)
θ_c	Immersion-angle range of the cutting tool (deg)
φ	Fiber-orientation angle (deg)
φ_a	Absolute fiber-orientation angle (deg)
f_d	Feed direction (deg)
F_t, F_r	Tangential cutting force (N), radial cutting force (N)
dF_t, dF_r	Differential tangential cutting force (N), differential radial cutting force (N)
F_x, F_y	Milling force in x-direction (N), milling force in y-direction (N)
K_t, K_r	Tangential specific cutting force (N/mm^2), radial specific cutting force (N/mm^2)
h	Chip thickness (mm)
a	Axial depth of cut (mm)
da	Differential axial depth of cut (mm)
f_t	Feed rate (mm/rev-tooth)
R	Cutting-tool radius (mm)
ρ	Run-out error (mm)
λ	Run-out error angle (deg)
F_{res}	Resultant cutting force (N)
N_t	Number of teeth on the cutting tool
F_{sum}	Sum of the resultant cutting forces (N)

✉ Seung-Han Yang
  syang@knu.ac.kr

1 Advanced Cutting Tool Center, Daegu Mechatronics & Materials Institute, 3, Seongseogongdan-ro, Dalseo-gu, Daegu 42715, Republic of Korea

2 School of Mechanical Engineering, Kyungpook National University, 80, Daehak-ro, Buk-gu, Daegu 41566, Republic of Korea

1 Introduction

Carbon-fiber-reinforced plastics (CFRPs) exhibit excellent strength-to-weight ratios, thereby enhancing fuel efficiency in the transportation field. CFRPs constitute more than

50% of the weight of the B787 aircraft [1, 2]. Given the expanding use of CFRPs, the demands imposed on machining are rising [3–5]. Various CFRP manufacturing methods are actively being studied for use in civil and infrastructure applications [6, 7]. Cutting CFRP is problematic: anisotropy attributable to the fiber-orientation angle, and carbon-fiber and matrix inhomogeneities, can cause delamination, splintering, and fiber pullout during cutting [8, 9]. Excessive cutting-tool wear is also a serious issue [10]. Orthogonal cutting tests have been used to analyze such characteristics, which found that fiber-orientation angles critically affect cutting characteristics [11–16].

Although many studies have investigated CFRP cutting-force optimization, they had some limitations. First, in terms of cutting-force models, most studies have focused only on cutting force prediction, rather than the use of cutting-force models. Since no cutting-force model is currently employed for stabilization of CFRP cutting, one is needed. Second, studies to lower the cutting force via re-design of cutting tools and addition of further processes are ongoing. However, such studies (e.g., focusing on cutting-tool design) are challenging to conduct in the field. Third, studies have adopted a trial-and-error approach when changing the cutting conditions because the initial tool path was experimentally derived under limited conditions, i.e., a single radial depth of cut. Fourth, the addition of new processes increases costs, and optimization remains challenging.

To determine the necessary machine-tool power and rigidity of the cutting tool and fixtures, reliable modelling of the cutting force is important [17–20]. Efforts to stabilize the cutting process using dynamic modeling of both the machine and cutting tools are underway [21, 22]. Several cutting-force models have been proposed for CFRP milling [23–31] and drilling [32–35]. Kalla et al. [23] modeled the mechanistic cutting force of a helical end mill for CFRPs. The specific cutting force was derived through orthogonal cutting tests and then applied to oblique-cutting-force prediction; agreement with the experimental results was found. Karpat et al. [24] modeled specific cutting forces as simple sine functions of the fiber cutting angle through unidirectional CFRP milling tests. Multidirectional CFRP milling cutting forces were then predicted using this specific cutting-force model; the results were in good agreement with the experimental data. An attempt was made to predict cutting forces during double-helix angle milling [25]. Sheikh-Ahmad and Yadav [26] used regression analysis to model specific cutting forces. They predicted the cutting forces when milling unidirectional and multidirectional CFRPs. Sheikh-Ahmad et al. [27] used multiple regression analysis and a committee neural network in a specific-cutting-force model of cutting forces when milling CFRPs and concluded that the committee neural network was better than multiple regression analysis. Xiao et al. [28] derived the specific cutting force

as a function of the equivalent chip thickness and fiber orientation, and predicted milling cutting forces for multidirectional CFRPs. They confirmed that reducing the flank contact force reduced the surface roughness and flank wear. Ning et al. [29] predicted the average milling cutting force for multidirectional CFRPs based on the segmented specific cutting force. Wang et al. [30] confirmed that the peak cutting force varied periodically, and frequency–response functions were used to derive the dynamics of the workpiece and predict cutting-force fluctuations. Mullin et al. [31] proposed a method to derive specific cutting force using the average milling force, and verified their technique. Karpat et al. [32] predicted the cutting force of a double-point-angle polycrystalline diamond (PCD) drill. The thrust force and torque were used to derive the specific cutting force and edge coefficient. Seo et al. [33] characterized the chisel-edge region as an extrusion and predicted drilling cutting force by assuming that the lip was a small orthogonal element. Mai et al. [34] used the geometric angle of the drill to predict the cutting force. Wang et al. [35] used an artificial neural network and a genetic algorithm to derive the specific cutting force and predict the drilling cutting force. These models used numerical analysis to derive the cutting forces of solid cutting tools such as the drills and end mills employed for machining CFRPs. The specific cutting force for CFRPs changes continuously depending on the fiber orientation, the cutting-tool rotation angle, and geometry. The specific cutting force has been expressed as a polynomial or simple sine function of the fiber cutting angle. Some studies have sought to derive specific-cutting-force models using neural networks and machine learning [23, 27, 35].

Many studies have sought to stabilize the cutting force and ensure cutting quality by modifying the design of the cutting tool, fiber-orientation angle, and other parameters [3, 36–44]. Some have focused on cutting tools that reduce and stabilize the cutting force [36–39]. Chatelain and Zaghbani [36] compared cutting forces among three milling-tool geometries. They confirmed that a compressive thrust force was generated in a crossed helical milling tool, and fluctuations in the thrust force and feed force were reduced using a groove milling tool. Kwon et al. [37] analyzed thrust forces to design a step-drill geometry and confirmed that delamination could be reduced by reducing the thrust force. Wang et al. [38] analyzed the burr-formation and fracture modes associated with the edge radius of a milling tool. They confirmed that a small edge radius and shallow radial cutting depth could reduce burr generation. Ashworth et al. [40] identified various contributory factors and applied analysis of variance to cutting-tool geometry and machine tools. Others have performed in-depth analyses of milling-tool cutting characteristics for all CFRP orientation angles [38, 41–43]. Geier [43] determined the fiber-orientation angle at which

the cutting force was minimized under a specific cutting condition. Hosokawa et al. [44] used inclination milling to reduce the axial cutting force imparted by the helix angle, thus improving the quality of CFRP milling at high helix angles. Both of these studies [43, 44] focused on minimizing the cutting force by modifying the tool path. Although previous research [36–38, 40–44] contributed significantly to the stabilization of cutting forces and cutting quality, the results are applicable only under certain conditions because they were based on experiments. Additionally, these previous studies focused on factors that cannot be controlled during the cutting process, such as the cutting-tool geometry and machine-tool rigidity.

Some studies have attempted to stabilize the cutting force via workpiece preheating, ultrasonic vibration, or cryogenic machining [45–47]. Kim et al. [45] confirmed that preheating CFRP reduced the thrust force and tool wear, as the epoxy was softened prior to drilling. Wang et al. [46] found that elliptical ultrasonic vibration reduced the cutting force in the feed direction, and Morkavuk et al. [47] found that cryogenic machining reduced delamination and damage to the machined surface. However, these methods are expensive and must be optimized, such that field application is currently difficult.

In contrast, we present an efficient method for determining the optimal feed direction to minimize the cutting force.

The method can be efficiently adopted for G-code generation in the field, even when the cutting-tool geometry and workpiece shape are fixed. Also, the cutting-force-prediction model can be used under various cutting conditions.

We first analyzed the relative angle between the cutting tool and the CFRP. Because the fiber cutting angle has the most significant effect on the cutting characteristics, we explored how engineers might easily change that angle during cutting. We built an algorithm that uses the cutting-force model to find the feed direction that minimizes the cutting force. Face-milling experiments employing a PCD tool were conducted to verify the method, which confirmed that the cutting force stabilized and productivity improved, indicating that the model is efficient.

2 Model approach and experimental procedure

2.1 Optimal milling feed direction model

When milling CFRPs using a solid cutting tool, i.e., a face mill or an end mill, the angle of interaction between the fiber and the cutting-tool teeth changes continuously due to the cutting-tool rotation angle (θ) and the fiber-orientation angle (φ) (Fig. 1). It is difficult to analyze cutting characteristics
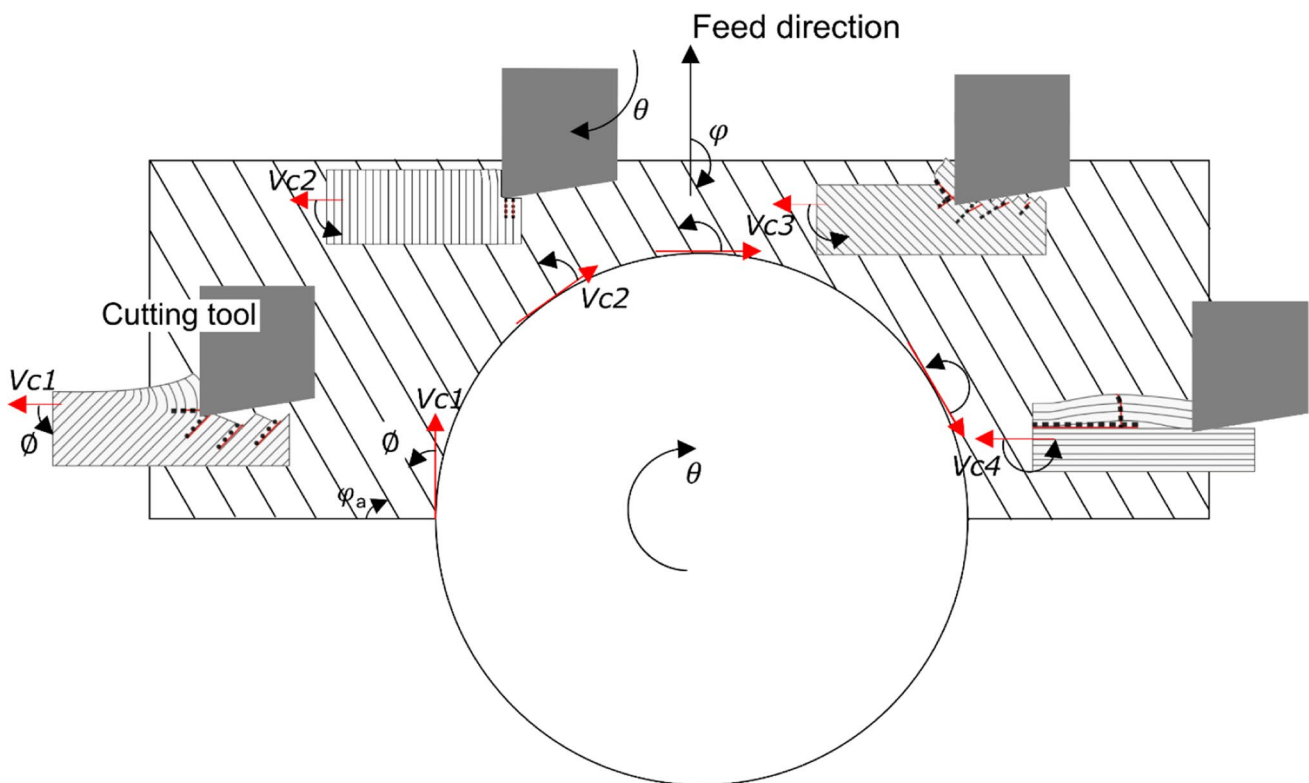

Fig. 1 Variation in the fiber cutting angle with the cutting-tool rotation angle

based on these angles, which significantly affect the cutting force. Therefore, a detailed analysis of these angles is required, although this is challenging for milling tools. It is nonetheless important to understand the relationship between the rotation angle of the cutting tool and the fiber cutting angle by researching orthogonal cutting.

Figure 2 presents the relationships between the fiber-orientation angle, the cutting-tool rotation angle, and the cutting force. The absolute fiber-orientation angle (φ_a) is the angle that the fiber makes (in a clockwise direction) with the x-direction of the Cartesian co-ordinate system. This varies with the shape of the CFRP and the location of the CFRP on the machine-tool table. The fiber-orientation angle (φ) is the angle the fiber makes (in a clockwise direction) with the feed direction (f_d). This angle varies with the feed direction. The angle of interaction between the cutting-tool teeth and the fiber is the fiber cutting angle ($\varnothing$), thus the angle the fiber makes (in the counterclockwise direction) with the tangent to the cutting-tool teeth.

The cutting forces F_t, F_r (in cylindrical co-ordinates) generated during milling can be expressed as F_x, F_y values via co-ordinate transformation.

The range of the fiber cutting angle depends on the cutting-tool rotation angle and the fiber-orientation angle.

$$\varnothing = (\theta - \varphi) + 180° \; for -180° < \theta - \varphi \le 0°$$
$$\varnothing = (\theta - \varphi)° \; for \; 0° < \theta - \varphi < 180° \tag{1}$$

The entry angle (θ_S) is a function of the radial depth of cut (R_d) and the cutting-tool diameter (D). The exit angle (θ_E) is the angle at which the teeth of the cutting tool exit the workpiece after cutting, and θ_c is the immersion angle of cutting-tool rotation [17].

$$\theta_E = 180°$$
$$\theta_S = 180° - \left\{ \left(arc \cos \left(1 - \frac{R_d}{D} \right) \times \frac{180}{\pi} \right) \right\} \tag{2}$$
$$\theta_C = \theta_E - \theta_S$$

The cutting-force model is a mechanistic model that divides the axial depth of cut and cutting-tool rotation angle into the axial lengths and rotation angles of a finite number of disks. The cutting forces applied to each disk are calculated using Eq. (3) [48, 49]. As orthogonal cutting is assumed, the model addresses only the tangential and radial cutting forces, and not the axial force. K_t, K_r are the tangential and radial specific cutting forces required to remove a unit chip, respectively. dF_t, dF_r are the differential tangential and radial cutting forces acting on a disk, respectively, and da is the differential disk length of axial depth.

$$dF_t = K_t h da$$
$$dF_r = K_r h da \tag{3}$$

For a metal, it can be assumed that the specific cutting force is the same in all feed directions; these values can be derived easily via experiments. However, as discussed above, CFRP cutting forces differ according to the fiber cutting angle. Thus, derivation of specific cutting forces is needed for milling tools. We derive the specific cutting forces using Eq. (4). The tangential and radial cutting forces of Eq. (4) are experimental values.

$$K_t = \frac{dF_t}{h da}$$
$$K_r = \frac{dF_r}{h da} \tag{4}$$

Fig. 2 Schematic showing the interactive angles and the cutting force between the cutting tool and the CFRP during milling
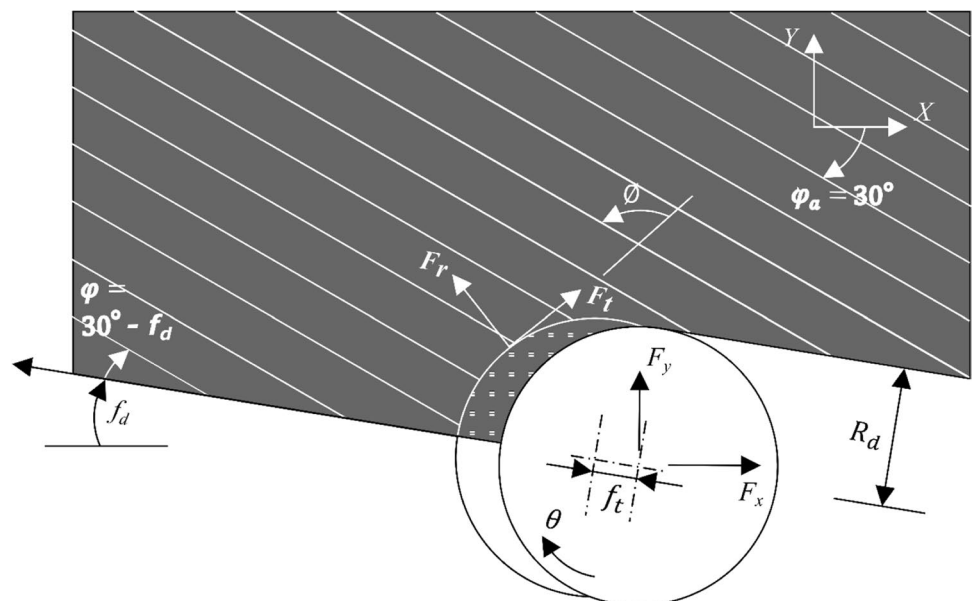
We ignore rubbing effects that reflect tool wear and edge chipping because we use a laser to sharpen the tool continuously [23].

The chip thickness and area can be expressed as Eq. (5), where h is the chip thickness based on the cutting-tool rotation angle and hda is the area of the chip. f_t is the feed rate (mm/rev-tooth).

$$h = f_t \sin\theta$$
$$hda = f_t \sin\theta \cdot da \tag{5}$$

Run-out error occurs when the center of rotation of the cutting tool differs from that of the spindle or tool holder [49]. Although the cutting tool per se may be in error, this can be ignored because the error is included in the other two errors mentioned above. The radius of rotation of the cutting tool changes on run-out; the chip thickness removed by each tooth differs. Equation (6) provides the changes in the cutting-tool radius (R) and chip thickness based on the run-out: here, ρ is the run-out error in the horizontal direction, and λ is the run-out error angle.

$$R_j(k) = R + \rho \cos\left[\delta\lambda - \lambda + (k-1)\frac{2\pi}{N_t}\right]$$
$$h_j(k) = R_j(k) - R_j(k-1) + f_t \sin\theta \tag{6}$$

Figure 3 presents the changes in chip thickness based on run-out [Eq. (6)]. Figure 3a shows the chip thickness when the run-out is 0 and Fig. 3b shows that when ρ is 2 μm and λ is 0. When run-out occurs, the chip thickness fluctuates from 0.023–0.027 mm, which causes large fluctuations in the cutting force depending on the depth of cut. Differences in the chip thickness of each tooth change the cutting force and induce fluctuations in surface roughness. In severe cases, the wear of a specific tooth is accelerated. While efforts are made to eliminate run-out in machining, complete elimination is impossible. Therefore, it is necessary to assess differences in the cutting forces applied to the teeth by predicting the changes in the cutting force when run-out occurs.

The tangential and radial cutting forces on a disk [Eq. (3)] can be transformed into Cartesian co-ordinates:

$$\begin{bmatrix} dF_x \\ dF_y \end{bmatrix} = \begin{bmatrix} \cos\theta & \sin\theta \\ -\sin\theta & \cos\theta \end{bmatrix} \begin{bmatrix} dF_t \\ dF_r \end{bmatrix} \tag{7}$$

The final cutting force is calculated by summing the forces imparted by all teeth of a disk [Eq. (8)]; F_{res} is the resultant cutting force. The cutting-tool tooth-index number is k, and the number of cutting-tool teeth is N_t. The number of disks that are axially sliced is l, and the index number of the axial disk is j.

$$F_x = \sum_{k=1}^{N_t}\sum_{j=1}^{l} dF_{x_{kj}} \quad F_y = \sum_{k=1}^{N_t}\sum_{j=1}^{l} dF_{y_{kj}} \quad F_{res} = \sum_{k=1}^{N_t}\sum_{j=1}^{l} \sqrt{dF_{x_{kj}}^2 + dF_{y_{kj}}^2} \tag{8}$$

As mentioned above, the fiber cutting angle significantly affects the cutting characteristics. A change in the angle thus also influences the cutting characteristics. Because the fiber cutting angle is a function of the fiber orientation and cutting-tool rotation angles during milling (Fig. 1), these angles must be changed when the cutting characteristics need to be changed. The immersion angle range of cutting-tool rotation is a function of the radial depth of cut and the cutting-tool diameter. The fiber-orientation angle is a function of the feed direction and the absolute fiber-orientation angle. Table 1 lists these relationships.

The parameters in Table 1 must be adjusted when the cutting characteristics are to be changed. During milling, some parameters are determined by the part to be milled and the location of machining, and these parameters are difficult to vary. The absolute fiber-orientation angle and the cutting-tool diameter are determined by the design of the part and the required cutting process, but the feed

Table 1 Parameters affecting the fiber cutting angle

Angle	Related parameter
∅	$f(\theta_C, \varphi)$
θ_C	$f(D, R_d)$
φ	$f(f_d, \varphi_a)$

Fig. 3 Chip thickness based on run-out: cutting-tool diameter 20 mm, Rd 10 mm, **a** $\rho = 0$ μm, $\lambda = 0$. **b** $\rho = 2$ μm, $\lambda = 0$
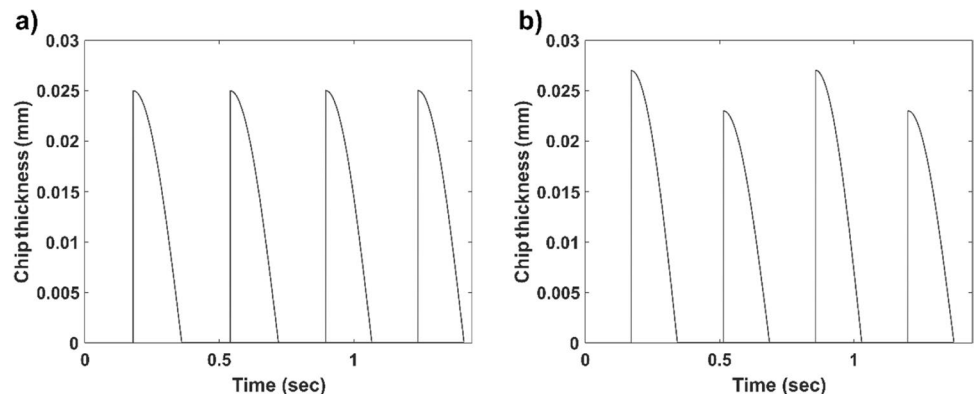
direction and the radial depth of cut can be changed easily. However, the latter affects the material removal rate and the cycle time; this parameter thus cannot be greatly reduced. In short, only the feed direction can be adjusted easily to change the fiber cutting angle in the cutting process. In particular, the feed direction in face milling can be modified easily because such milling only removes chips; no specific shape is encountered.

Experiments can yield an optimal feed direction, but simulation is preferable: if experiments are performed under limited conditions, more trial-and-error experimentation is required when the conditions change. We use a cutting-force model to adjust the feed direction to minimize the cutting force. Figure 4 shows the process of determining the optimal feed direction. The red box in Fig. 4 represents the cutting-force model. Feed
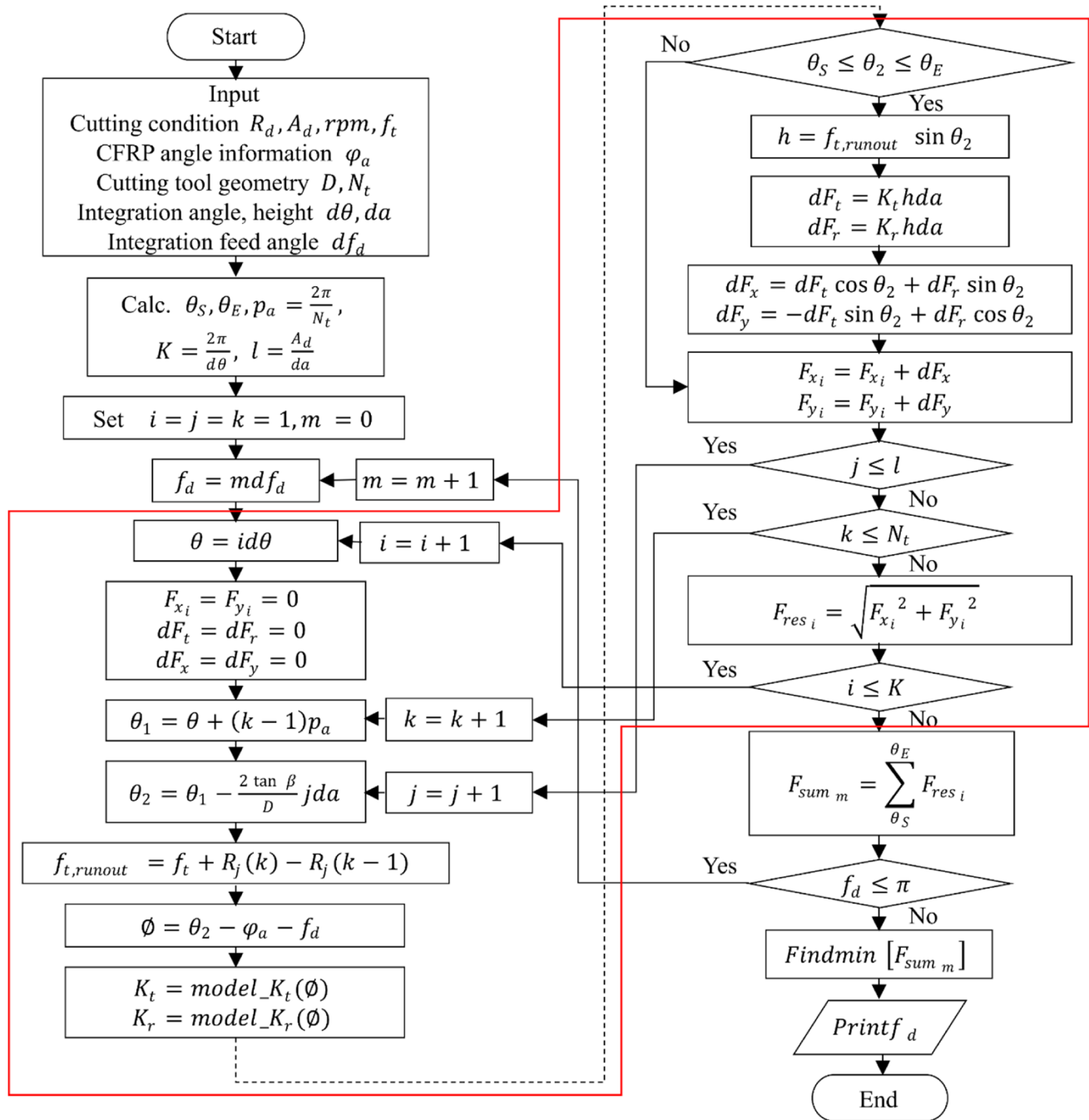

Fig. 4 Flowchart for detecting the feed direction that minimizes the cutting force

directions of 0–180° are repeatedly input into the model, which derives the cutting force for each feed direction (m) and compares the sum of the resultant cutting forces (F_{sum}). The optimal feed direction is that for which F_{sum} is lowest.

The milling feed may be a straight line in one direction or in two directions (zigzag) depending on the characteristics of the material and the condition of the workpiece. We consider only a straight line in one direction.

2.2 Experiments

In the milling test, we used a CFRP with six different absolute fiber-orientation angles: 0, 30, 60, 90, 120, and 150°. The plate thickness was 10 mm and each prepreg thickness was 0.137 mm. Table 2 lists the properties of the CFRP.

The CFRP was fixed to a tool dynamometer (Fig. 5a). A vertical machining center (Doosan NX6500II, maximum rpm 20,000) was used (Fig. 5b). The cutting tool was a 20-mm-diameter, two-tooth, flat PCD milling tool.

Table 2 Properties of the CFRP

Property	Value
Carbon/resin weight (g/m^2)	150/64
Prepreg thickness (mm)	0.137
Tensile strength (MPa)	653
Tensile modulus (MPa)	58
Flexural strength (MPa)	806
Flexural modulus (GPa)	74.63

The Illjin CFW PCD features a diamond grain size of 4 μm and is manufactured by brazing PCD onto a tungsten-carbide (WC) body. The edge of the cutting tool was prepared using a nano-pulsed laser (DMG MORI Lasertec 20). The edge radius was maintained at under 6 μm via laser treatment prior to every test. The clearance angle of the PCD tool was 20° and the rake angle was 0° (Fig. 5c). The cutting forces in the x, y, and z directions were measured using a Kistler 9119AA2 tool dynamometer operating at 5000 Hz. A low-pass filter (2000 Hz) and a moving-average filter were used to remove high frequencies (Fig. 5d). All experiments were conducted under dry conditions, and dust was removed using a vacuum cleaner.

Table 3 lists the cutting conditions. The specific-cutting-force data were collected at 2547 rpm (cutting speed = 160 m/min), a feed rate of 127.3 mm/min (0.05 mm/rev), and radial and axial depths of cut of 10 and 1 mm, respectively. The cutting-force model was validated by measuring the cutting forces associated with a radial depth of cut in the range 2–10 mm at each fiber-orientation angle. The optimal feed direction was tested at 1615 rpm (cutting speed 100 m/min), with a feed rate of either 161 or 350 mm/min, up to radial and axial depths of cut of 2 and 5 mm, respectively. All cutting speeds were below 160 m/min, because faster cutting speeds introduce other effects on the cutting force [23, 24, 50]. The CFRP cutting force varies depending on the depth of cut, fiber-orientation angle, feed rate, and cutting-tool diameter. As it was not possible to consider all changes experimentally, partial conclusions were obtained based on previous studies; each parameter was fixed in the experimental studies.

Fig. 5 CFRP cutting-force measurements (the experimental setup). **a** Fixture. **b** Machine tool. **c** PCD cutting tool. **d** Filtering of the measured force
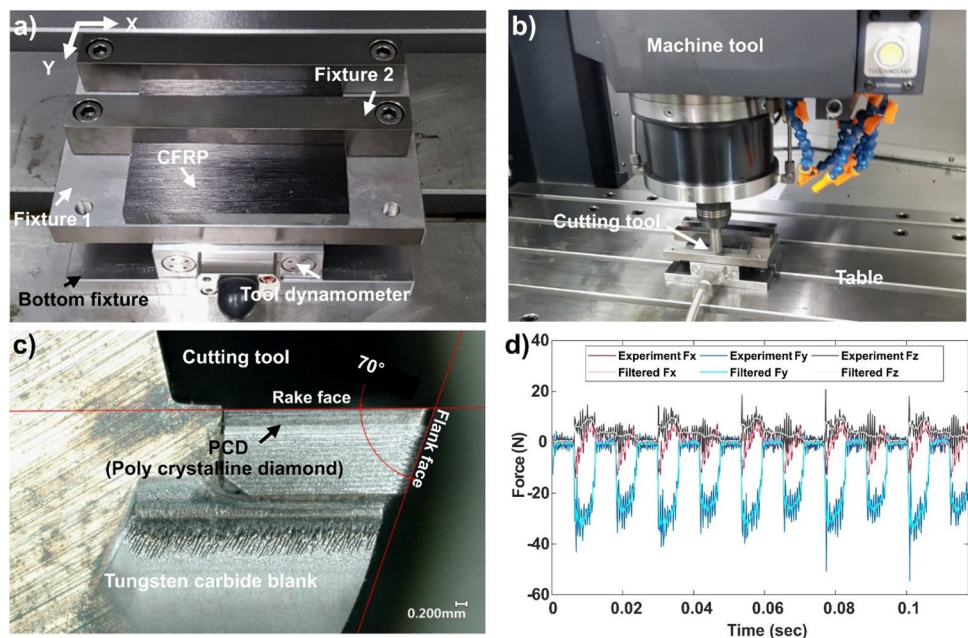
Table 3 Cutting conditions during milling

Parameter	Specific-cutting-force derivation	Cutting-force model validation	Optimal-feed-direction validation
Rotational speed (rpm)	2547	2547	1615
Cutting speed (m/min)	160	160	100
Feed rate (mm/min)	127.3	127.3	161 or 350
Radial/axial depth of cut (mm)	10/1	(2, 4, 6, 8, 10)/1	2/5
Cutting tool	Diameter 20 mm, two-tooth PCD milling tool	Diameter 20 mm, two-tooth PCD milling tool	Diameter 19.7 mm, two-tooth PCD milling tool
Material and fiber-orientation angle	UD CFRP 0, 30, 60, 90, 120, 150°	UD CFRP 0, 30, 60, 90, 120, 150°	UD CFRP 0°

However, we propose a model-based simulation method. Although changes in cutting speed can affect the specific cutting force, the effect is minimal compared to those of the depth of cut, fiber-orientation angle, feed rate, and cutting-tool diameter.

3 Results and discussion

3.1 Specific cutting force

To derive the specific cutting forces, the cutting forces (in Cartesian co-ordinates) were transformed to cylindrical co-ordinates. Figure 6 presents the cutting forces and chip areas (yellow line) based on the fiber-orientation angle. During down milling, the chip area was largest at the entry angle of the cutting tool, and was 0 at the exit angle. Therefore, the cutting force was generally largest at the entry angle (in proportion to the chip area) and 0 at the exit angle. However, at fiber-orientation angles of 30°, 60°, and 90°, the cutting forces differed from the theoretical values. For these fiber-orientation angles, the fiber cutting angles were 60–150°, 30–120°, and 0–90°, respectively. The specific cutting forces in these ranges differed from the changes in chip thickness, as shown in Fig. 7.

The immersion-angle range of the cutting tool is 90–180° when the radial depth of cut is 0.5 D. To eliminate cutting-force instability around the entry angle and the size effect around the exit angle, specific cutting forces were derived at cutting-tool rotation angles of 100–120° in 10° units. Signal processing using a low-pass, moving-average filter removed unpredictable errors, but high-frequency fluctuations remained. The specific cutting forces were derived by measuring the forces during four rotations of the cutting tool; this reduced the errors.

Figure 7 presents the specific cutting forces for each fiber cutting angle. In the tangential direction, the specific cutting force decreased at fiber cutting angles of 0–40°, increased up to a fiber cutting angle of 60°, remained at this value to 140°, and then decreased to a fiber cutting

angle of 180°. In the radial direction, the specific cutting force decreased at fiber cutting angles of 0–30° and then increased at angles of up to 130°.

At a fiber cutting angle of 0°, severe fiber buckling occurred because the rake angle of our cutting tool was 0°. When the fiber cutting angle was greater than 0°, the tooth applied pressure to the fiber in the direction of the cut, and the fibers peeled away from the matrix. The fractures were a mix of mode-I and mode-II fractures. At a fiber cutting angle of 40°, the specific cutting force was less than that at 0° because mode II was dominant. When the fiber cutting angle was in the range 45–90°, fiber delamination and interlaminar shear forces between the fiber and matrix caused severe deformation. Extensive elastic bending occurred because of compression at the cutting edge, resulting in cracks and long discontinuous chips. Elastic recovery occurred as the fiber was cut, producing fluctuations in the cutting force and increasing the variance in the tangential direction. At fiber cutting angles in the range 90–130°, the fiber contacted the rake face rather than the tooth edge because the cutting-tool rake angle was 0°. At fiber cutting angles in the range 130–165°, chipped segments slid up the rake face, similar to metal cutting. However, elastic recovery developed at the machined surface, which led to fiber contact with the flank face of the cutting tool, and an increased radial specific cutting force. These results agree well with the literature in terms of chip formation and make it possible to understand chip formation using a milling tool [11, 15, 16].

For CFRP cutting, a specific-cutting-force model must reflect changes in the force at all fiber cutting angles and at high sampling rates; some studies have used a simple sine function or machine learning to this end. However, we used regression, because this is straightforward. We employed tenfold cross-validation to create and validate the regression [51]. We found the polynomial order that minimized the root mean square error (RMSE): a satisfactory RMSE was obtained at order 6 (Eq. (9)).

$$K_t = 1012.3 - 4731.1\varnothing + 10408\varnothing^2 - 9320.5\varnothing^3 + 4410.6\varnothing^4 - 1100.7\varnothing^5 + 112.5\varnothing^6$$

$$K_r = 1207.7 - 6852.5\varnothing + 16852\varnothing^2 - 18917\varnothing^3 + 10745\varnothing^4 - 2930.3\varnothing^5 + 303.4\varnothing^6 \quad (9)$$

Fig. 6 Chip areas and cylindrical co-ordinates of the cutting forces at various fiber-orientation angles: **a** $\varphi = 0$ °, **b** 30 °, **c** 60 °, **d** 90 °, **e** 120 °, and **f** 150 °
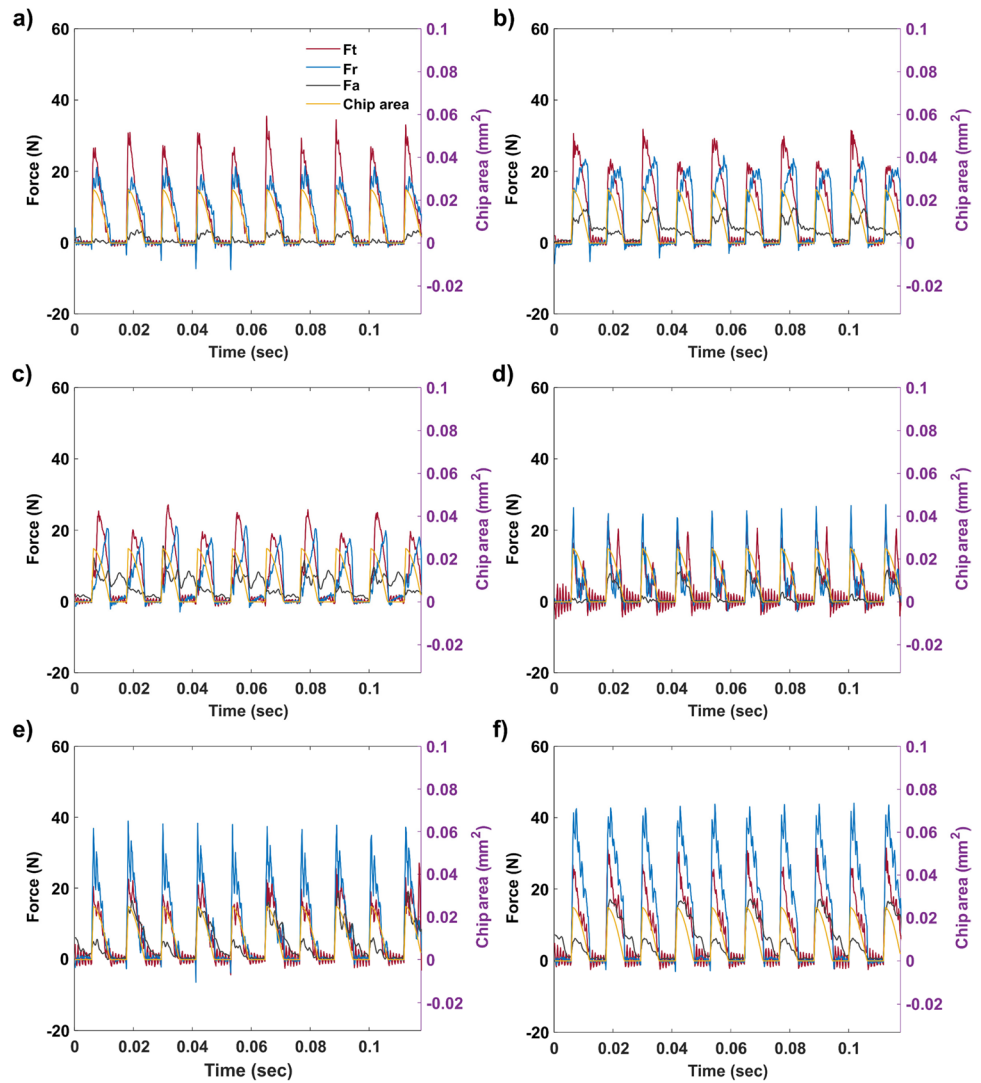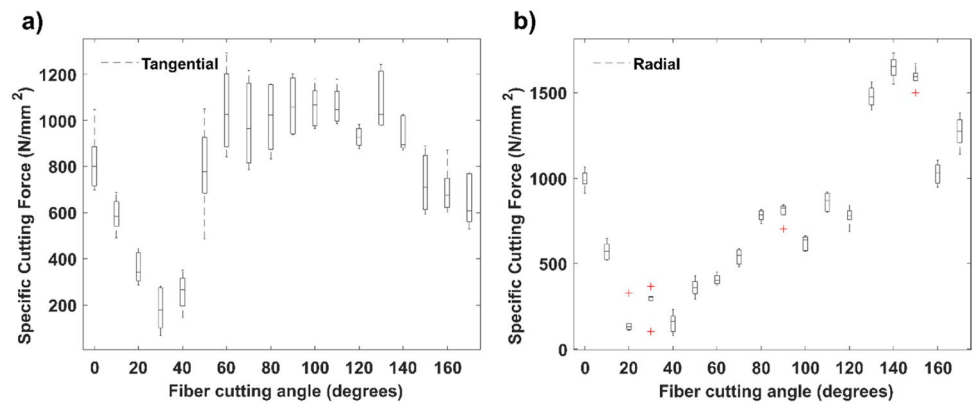

Fig. 7 Specific cutting forces by the fiber cutting angle. **a** Tangential direction. **b** Radial direction

3.2 Cutting-force-model validation

The predicted and experimental cutting forces were compared by the radial depth of cut at each CFRP orientation angle to verify the model (red box in Fig. 4). At each of the five tested fiber-orientation angles, the cutting-force predictions were verified at five radial depths (0.1, 0.2, 0.3, 0.4, and 0.5 D [diameter]) of cut; the experimental and predicted values were in good agreement. Some representative results of the prediction are shown in Fig. 8.
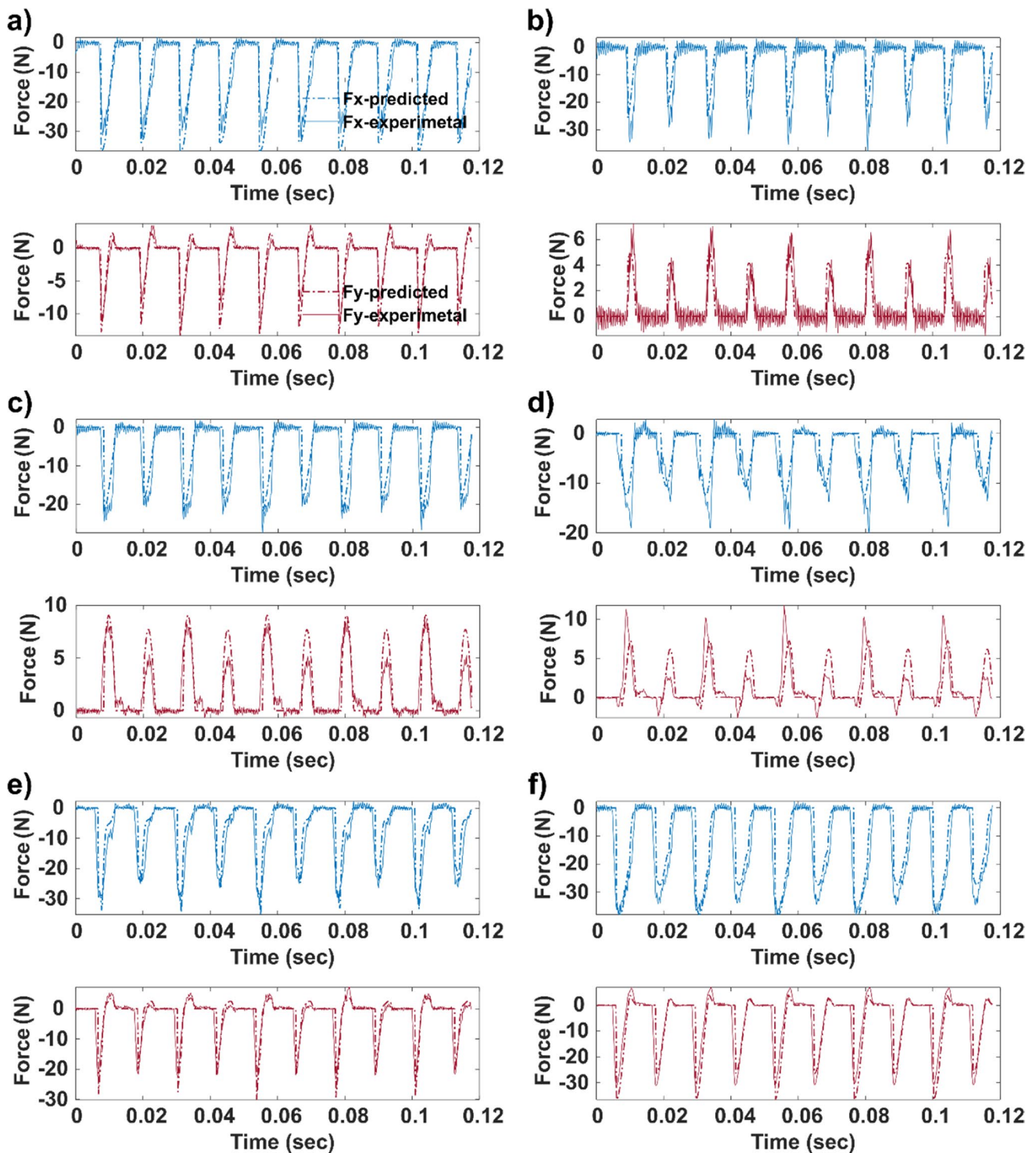
Fig. 8 Comparison of real (experimental) and predicted forces: 2547 rpm, 127 mm/ min, A_d 1 mm: **a** R_d 6 mm, φ 0°, **b** R_d 2 mm, φ 30°, **c** R_d 4 mm, φ 60°, **d** R_d 6 mm, φ 90°, **e** R_d 8 mm, φ 120°, **f** R_d 10 mm, φ 150°

The cutting forces predicted by our model, and those obtained under the same cutting conditions in the literature, are shown in Fig. 9 [43]. A 50-mm-diameter cutting tool was used to make radial and axial depths of cut of 3 and 7 mm, respectively. Although the CFRP properties and cutting tool differed from those described in the literature, the relationship between the cutting force and the fiber-orientation angle was similar. The fiber-orientation angle for the minimum
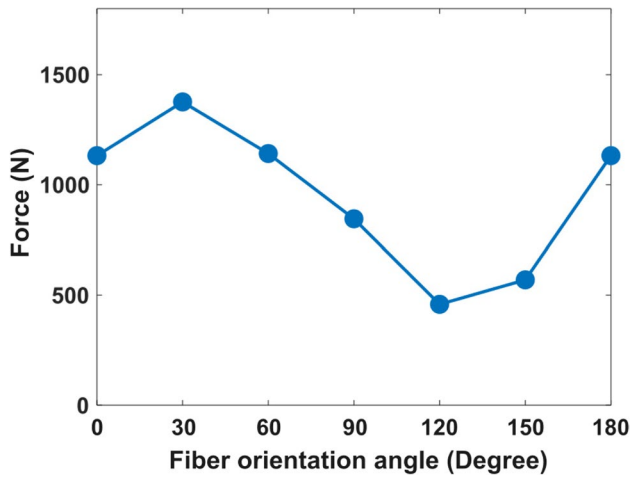
Fig. 9 Predictions of resultant cutting forces based on fiber-orientation angles: 1464 rpm, 397 mm/min, A_d 7 mm; R_d 3 mm, cutting-tool diameter 50 mm, N_t 5

cutting force (120°) was identical to those reported in the literature. The cutting-tool specifications and changes in cutting speed significantly affected the quality of the cut [11, 42]. However, many predictive cutting-force models do not consider the tool geometry or cutting speed. If these factors are not extreme, they affect only the offset of the cutting force magnitude, and not the maximum and minimum force with respect to fiber orientation. Thus, the specific cutting forces reported in several studies were derived using different conditions but demonstrated similar characteristics [24, 26, 31]. Therefore, when CFRP-specific cutting-force

data are available, cutting-force trends under various conditions can be estimated using the cutting-force model. As our method is not experimental, it is possible to derive the optimal feed direction efficiently with minimal experimentation, even when the shape of the cutting tool changes.

3.3 Optimal milling feed direction validation

Figure 10 presents the optimal feed direction derived using the steps in Fig. 4. The optimal feed direction should be derived, after the CFRP workpiece has been fixed on the machine tool in an arbitrary direction in terms of the absolute fiber-orientation angle. First, the fiber-orientation angle that minimizes the cutting force is derived, as shown in Fig. 10. The optimal feed direction is calculated by Eq. (10).

$$\varphi_a - f_d = \varphi$$
$$f_d = \varphi_a - \varphi \tag{10}$$

The range of fiber cutting angles changes with the radial depth of cut, as shown in Fig. 2, so the optimal feed direction depends on that depth. Figure 10a presents $\sum F_{res}$ values based on changes in the feed direction when the radial depth of cut increases from 1 mm to the diameter (20 mm) of the cutting tool. As might be expected, as the depth increases, the cutting force rises, as does $\sum F_{res}$. The cutting forces differ greatly with the feed direction. Since the optimal feed direction can lower the cutting force, the MRR can be increased by increasing the radial depth of cut. Figure 10b presents the feed directions associated with the lowest cutting forces for each radial depth of cut. The optimal feed direction decreases from approximately 140° to
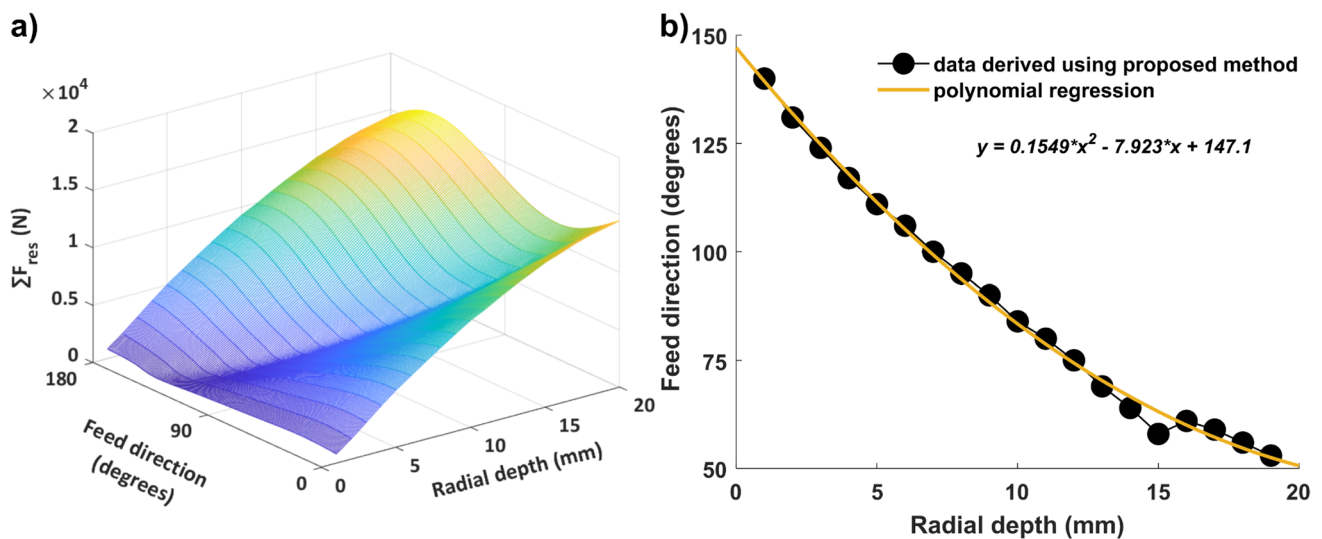

Fig. 10 Variations in the cutting force with the radial depth of cut and the feed direction. **a** The trend in $\sum F_{res}$. **b** Optimal feed direction as indicated by the R_d

50° as the radial depth of cut increases from 1 mm to slotting. If various CFRPs require machining, or if the optimal feed direction of various radial depths of cut must be determined quickly, the fitted curve (the orange line) obtained via regression analysis is useful.

Since the specification of the CFRP in this study was fixed, a specific-cutting-force database is needed to apply this method to various specifications of CFRP. However, when specific-cutting-force data are available, the optimal feed direction for various types of CFRPs can be determined using the proposed method, as shown in Fig. 10b.

When the $\sum F_{res}$ decreases are expressed as percentages of the maximum after determining the feed direction, the effect becomes greater as the radial depth of cut decreases (Fig. 11). The cutting-force reduction is more marked when using a cutting-tool path with a low radial depth of cut. Cutting-force optimization is generally used when roughing rather than during finishing. Cycle times or MRR is more important than cutting quality when roughing. A low feed rate or shallow depth of cut can significantly reduce the cutting force. However, these methods are not used for cutting-force optimization because they affect the cycle time or MRR. If quality is important, such as during finishing, machining is performed under stable conditions regardless of the cycle time; typically, the finishing radial depth of cut is low. Even though the effect of a reduction in CFRP cutting force is more significant when the radial depth of cut is low, it is important to consider cutting quality under finishing conditions such as a low radial depth of cut.

We performed face-milling tests to verify the data in Fig. 10. The first test was conducted prior to optimization of the feed direction; the absolute fiber-orientation angle of a CFRP specimen $70 \times 100 \times 5$ mm³ in volume was 0°, the horizontal feed direction ($\varphi = 0°$) was in play,
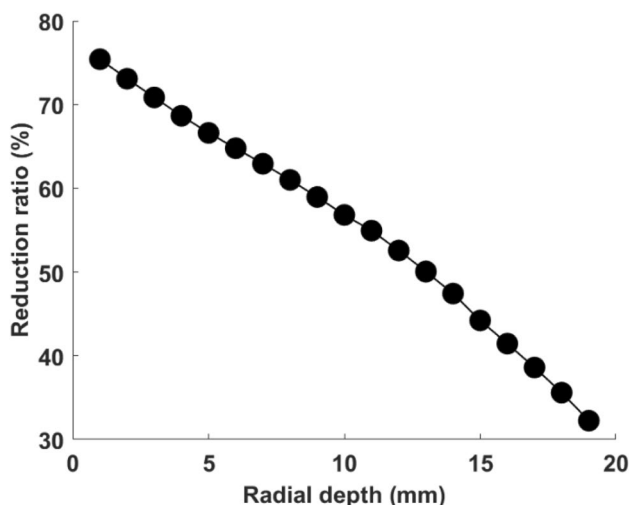

Fig. 11 Cutting force reduction ratio with radial depth of cut

this is a general method (Fig. 12a, top). The yellow line of the toolpath is the G01 path. Figure 12(a) presents the experimental cutting forces (middle) and the predicted forces (bottom). The maximum cutting force was approximately 280 N (both experimentally and predicted). We changed the feed direction to a fiber-orientation angle of 135° (the optimal feed direction; Fig. 10b) and compared the experimental (blue line in the top panel) and predicted (blue line in the bottom panel) cutting forces. The maximum experimental and predicted cutting forces were both approximately 145 N. After feed-direction optimization, the cutting forces decreased by more than 54% (based on the mean value), decreasing the burdens imposed on the cutting and machine tools, and the fixture. The cycle time was reduced by increasing the feed rate, because use of the optimal feed direction lowered the cutting force. The orange line in Fig. 12b shows the cutting forces when the feed rate was increased to reduce the cycle time. The feed rate was changed from 161 to 350 mm/min; the maximum cutting force then became similar to that prior to optimization. Removal of $70 \times 100 \times 5$ mm³ initially required 28 min at a feed rate of 161 m/min; after feed-direction optimization, it required 15 min at 350 m/min. It was thus possible to reduce the cycle time by at least 53% without changing the cutting force.

4 Conclusion

We present a method for determining the feed direction that minimizes the cutting force. We first confirmed that it is possible to change the fiber cutting angle, which significantly affects CFRP cutting characteristics, by modifying the feed direction. Our method uses a cutting-force model to determine the optimal feed direction. To verify this method, we used a PCD milling tool and found that the cutting force was well-stabilized. This method increases CFRP cutting efficiency; only the feed direction is changed. Using this predictive cutting-force model, the optimal feed direction under various cutting conditions can be derived with minimal experimentation. Our key findings are as follows.

The fiber cutting angle is expressed as a function of the absolute fiber orientation and the cutting-tool diameter, the feed direction, and the radial depth of cut. Of these parameters, only the feed direction is easy to vary; the other parameters are determined by the shape of the cut part. Our method minimizes the cutting force by changing the feed direction, which engineers can easily achieve. Feed directions from 0 to 180° are individually (and repeatedly) entered into the cutting-force model and analyzed. The optimal feed direction is then derived by summing the cutting forces in each direction. Because this method is
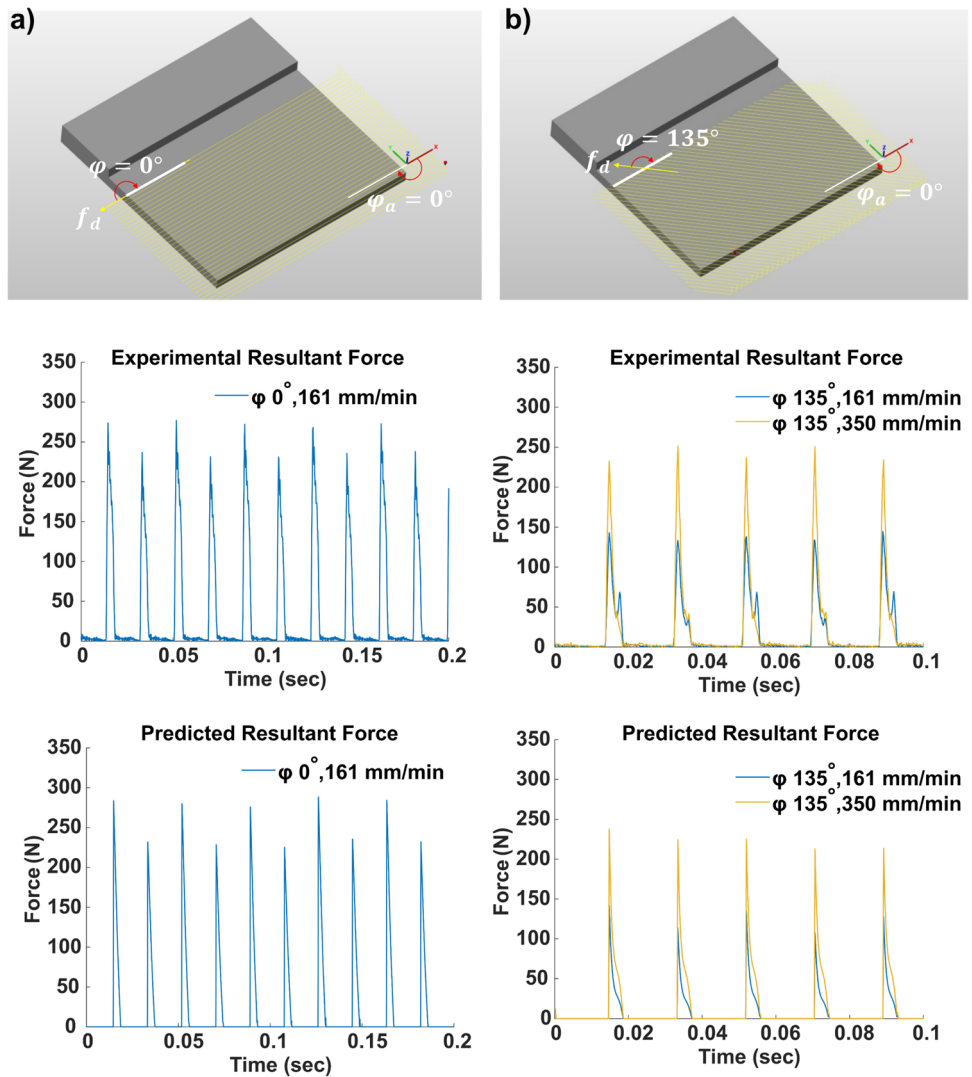
Fig. 12 Cutting force based on the optimized feed direction. **a** Before optimization. **b** After optimization. [Diameter 19.75 mm, R_d 2 mm, A_d 5 mm, 1,615 rpm : **a** φ 0°, 161 mm/min, **b** φ 135°, 161 mm/min (blue line), 350 mm/min (orange line)]

predictive rather than experimental, it is possible to determine the optimal feed direction efficiently under various cutting conditions, such as for different cutting-tool diameters, radial depths of cut, and fiber-orientation angles.

We used a mechanistic cutting-force model and derived the specific cutting force via regression. The predicted and experimental forces were in good agreement. If the specific cutting forces of various types of CFRPs are available, the optimal feed direction under various conditions can be determined, because even if the cutting-tool and CFRP specifications change, the trend in the cutting force based on the fiber-orientation angle is not dramatically affected.

The feed direction that minimizes the cutting force changes from 140 to 50° as the radial depth of cut increases from 1 mm to the diameter of the cutting tool.

Regression analysis allows the optimal feed direction to be expressed as a fitting curve. Because various cutting conditions require time to find the optimal feed direction, if there is no need to simulate the cutting-force details, the optimal feed direction can be determined using the fitting curve.

Our method was verified using PCD face-milling experiments. The cutting force was reduced by 54% and the feed rate could be increased. Finally, the cycle time could be reduced by 53% at the same cutting force. Therefore, use of our method to determine the optimal feed direction reduces the cutting force required for CFRPs, thereby improving productivity.

Cutting-force optimization is best used for roughing, when the cycle time or MRR is more important than cut

quality. Our method can efficiently reduce cutting forces during roughing. If CFRP cutting quality and defects are also to be considered, both cutting force and quality could be stabilized. Therefore, our future work will focus on optimizing the feed direction considering both cutting force and quality simultaneously.

Declarations

Conflict of interest The authors declare no competing interests.

Ethics approval Not applicable.

Consent to participate All authors agreed to participate.

Consent for publication All authors have agreed to manuscript submission.

References

1. Hale J (2012) Boeing 787 from ground up. Boeing Comer. Aeromagazine 9. https://www.boeing.com/commercial/aeromagazine/articles/qtr_4_06/article_04_2.html
2. Grzesik W (2017) Machinability of engineering materials. Adv Mach Process Met Mater 241–264. https://doi.org/10.1016/b978-0-444-63711-6.00013-2
3. Geier N, Xu J, Pereszlai C et al (2020) Drilling of carbon fibre reinforced polymer (CFRP) composites: Difficulties, challenges and expectations. Procedia Manuf 54:284–289. https://doi.org/10.1016/j.promfg.2021.07.045
4. Seo JW, Kim DY, Kim DC, Park HW (2021) Recent developments and challenges on machining of carbon fiber reinforced polymer composite laminates. Int J Precis Eng Manuf 22:2027–2044. https://doi.org/10.1007/s12541-021-00596-w
5. Geier N, Poór DI, Pereszlai C, Tamás-Bényei P (2022) Drilling of recycled carbon fibre–reinforced polymer (rCFRP) composites: analysis of burrs and microstructure. Int J Adv Manuf Technol 120:1677–1693. https://doi.org/10.1007/s00170-022-08847-4
6. Alajarmeh O, Zeng X, Aravinthan T et al (2021) Compressive behaviour of hollow box pultruded FRP columns with continuous-wound fibres. Thin-Walled Struct 168:108300. https://doi.org/10.1016/j.tws.2021.108300
7. Vedernikov A, Tucci F, Safonov A et al (2020) Investigation on the shape distortions of pultruded profiles at different pulling speed. Procedia Manuf 47:1–5. https://doi.org/10.1016/j.promfg.2020.04.107
8. Gemi L, Morkavuk S, Köklü U, Yazman Ş (2020) The effects of stacking sequence on drilling machinability of filament wound hybrid composite pipes: part-2 damage analysis and surface quality. Compos Struct 235. https://doi.org/10.1016/j.compstruct.2019.111737
9. Doğan MA, Yazman Ş, Gemi L et al (2022) A review on drilling of FML stacks with conventional and unconventional processing methods under different conditions. Compos Struct 297. https://doi.org/10.1016/j.compstruct.2022.115913
10. Han C, Bin KK, Lee SW et al (2021) Thrust force-based tool wear estimation using discrete wavelet transformation and artificial neural network in CFRP drilling. Int J Precis Eng Manuf 22:1527–1536. https://doi.org/10.1007/s12541-021-00558-2
11. Wang DH, Ramulu M, Arola D (1995) Orthogonal cutting mechanisms of graphite/epoxy composite. Part I: unidirectional laminate. Int J Mach Tools Manuf 35:1623–1638. https://doi.org/10.1016/0890-6955(95)00014-O
12. Ramulu M (1997) Machining and surface integrity of fibre-reinforced plastic composites. Sadhana 22:449–472. https://doi.org/10.1007/BF02744483
13. Wang DH, Ramulu M, Arola D (1995) Orthogonal cutting mechanisms of graphite/epoxy composite. Part II: multi-directional laminate. Int J Mach Tools Manuf 35:1639–1648. https://doi.org/10.1016/0890-6955(95)00015-P
14. Wang XM, Zhang LC (2003) An experimental investigation into the orthogonal cutting of unidirectional fibre reinforced plastics. Int J Mach Tools Manuf 43:1015–1022. https://doi.org/10.1016/S0890-6955(03)00090-7
15. Sheikh-Ahmad JY (2009) The machining of polymers composites. Springer New York, NY. https://doi.org/10.1007/978-0-387-68619-6
16. Kaneeda, T. (1989). CFRP cutting mechanism. In Proc. of 17th North American Manufacturing Research Conf. (Vol. 220).
17. Altintas Y (2012) Manufacturing automation: Metal cutting mechanics, machine tool vibrations, and CNC design. Manuf Autom. https://doi.org/10.1017/CBO9780511843723
18. Altintaş Y, Budak E (1995) Analytical prediction of stability lobes in milling. CIRP Ann Manuf Technol 44:357–362. https://doi.org/10.1016/S0007-8506(07)62342-7
19. Budak E (2006) Analytical models for high performance milling. Part I: Cutting forces, structural deformations and tolerance integrity. Int J Mach Tools Manuf 46:1478–1488. https://doi.org/10.1016/j.ijmachtools.2005.09.009
20. Kang G, Kim J, Choi Y, Lee DY (2022) In-process identification of the cutting force coefficients in milling based on a virtual machining model. Int J Precis Eng Manuf 23:839–851. https://doi.org/10.1007/s12541-022-00677-4
21. Wu J, Yu G, Gao Y, Wang L (2018) Mechatronics modeling and vibration analysis of a 2-DOF parallel manipulator in a 5-DOF hybrid machine tool. Mech Mach Theory 121:1339–1351. https://doi.org/10.1016/j.mechmachtheory.2017.10.023
22. Wu J, Ye H, Yu G, Huang T (2022) A novel dynamic evaluation method and its application to a 4-DOF parallel manipulator. Mech Mach Theory 168:104627. https://doi.org/10.1016/j.mechmachtheory.2021.104627
23. Kalla D, Sheikh-Ahmad J, Twomey J (2010) Prediction of cutting forces in helical end milling fiber reinforced polymers. Int J Mach Tools Manuf 50:882–891. https://doi.org/10.1016/j.ijmachtools.2010.06.005
24. Karpat Y, Bahtiyar O, Deer B (2012) Mechanistic force modeling for milling of unidirectional carbon fiber reinforced polymer laminates. Int J Mach Tools Manuf 56:79–93. https://doi.org/10.1016/j.ijmachtools.2012.01.001
25. Karpat Y, Polat N (2013) Mechanistic force modeling for milling of carbon fiber reinforced polymers with double helix tools. CIRP Ann Manuf Technol 62:95–98. https://doi.org/10.1016/j.cirp.2013.03.105
26. Sheikh-Ahmad J, Yadav R (2008) Model for predicting cutting forces in machining CFRP. Int J Mater Prod Technol 32:152. https://doi.org/10.1504/IJMPT.2008.018978
27. Sheikh-Ahmad J, He Y, Qin L (2019) Cutting force prediction in milling CFRPs with complex cutter geometries. J Manuf Process 45:720–731. https://doi.org/10.1016/j.jmapro.2019.08.009
28. Xiao J, Gao C, Ke Y (2018) An analytical approach to cutting force prediction in milling of carbon fiber reinforced polymer laminates. Mach Sci Technol 22:1012–1028. https://doi.org/10.1080/10910344.2018.1449214

29. Ning H, Zheng H, Zhang S, Yuan X (2021) Milling force prediction model development for CFRP multidirectional laminates and segmented specific cutting energy analysis. Int J Adv Manuf Technol 113:2437–2445. https://doi.org/10.1007/s00170-021-06690-7

30. Wang C, Zhang X, Zhai Z, Chen X (2022) Parametric prediction model and periodic fluctuation interpretation of unidirectional CFRP edge milling force. Compos Struct 287:115387. https://doi.org/10.1016/j.compstruct.2022.115387

31. Mullin R, Farhadmanesh M, Ahmadian A, Ahmadi K (2020) Modeling and identification of cutting forces in milling of carbon fibre reinforced polymers. J Mater Process Technol 280:116595. https://doi.org/10.1016/j.jmatprotec.2020.116595

32. Karpat Y, Bahtiyar O, Değer B, Kaftanoğlu B (2014) A mechanistic approach to investigate drilling of UD-CFRP laminates with PCD drills. CIRP Ann Manuf Technol 63:81–84. https://doi.org/10.1016/j.cirp.2014.03.077

33. Seo J, Banerjee N, Kim Y et al (2020) Experimental and analytical investigation of the drilling forces of the carbon fiber reinforced plastics including thermal effects. J Manuf Process 58:1126–1137. https://doi.org/10.1016/j.jmapro.2020.08.063

34. Mai D, Kwon BC, Ko SL (2019) Practical implementation of cutting-force model for step drill using 3D CAD data. CIRP Ann 68:85–88. https://doi.org/10.1016/j.cirp.2019.04.055

35. Wang Q, Jia X, Hu B, Xia W (2019) A mechanistic prediction model of instantaneous cutting forces in drilling of carbon fiber-reinforced polymer. Int J Adv Manuf Technol 103:1977–1988. https://doi.org/10.1007/s00170-019-03571-y

36. Chatelain JF, Zaghbani I (2012) A comparison of special helical cutter geometries based on cutting forces for the trimming of CFRP laminates. Int J Mech 6:52–59

37. Kwon BC, Mai NDD, Cheon ES, Ko SL (2020) Development of a step drill for minimization of delamination and uncut in drilling carbon fiber reinforced plastics (CFRP). Int J Adv Manuf Technol 106:1291–1301. https://doi.org/10.1007/s00170-019-04423-5

38. Wang F, Yin J, Ma J et al (2017) Effects of cutting edge radius and fiber cutting angle on the cutting-induced surface damage in machining of unidirectional CFRP composite laminates. Int J Adv Manuf Technol. https://doi.org/10.1007/s00170-017-0023-9

39. Gemi L, Morkavuk S, Köklü U, Gemi DS (2019) An experimental study on the effects of various drill types on drilling performance of GFRP composite pipes and damage formation. Compos Part B 172:186–194. https://doi.org/10.1016/j.compositesb.2019.05.023

40. Ashworth S, Fairclough JPA, Takikawa Y et al (2019) Effects of machine stiffness and cutting tool design on the surface quality and flexural strength of edge trimmed carbon fibre reinforced polymers. Compos A Appl Sci Manuf 119:88–100. https://doi.org/10.1016/j.compositesa.2019.01.019

41. Hintze Wolfgang W, Hartmann D, Schütte C (2011) Occurrence and propagation of delamination during the machining of carbon fibre reinforced plastics (CFRPs) - An experimental study. Compos Sci Technol 71:1719–1726. https://doi.org/10.1016/j.compscitech.2011.08.002

42. Voss R, Seeholzer L, Kuster F, Wegener K (2017) Influence of fibre orientation, tool geometry and process parameters on surface quality in milling of CFRP. CIRP J Manuf Sci Technol 18:75–91. https://doi.org/10.1016/j.cirpj.2016.10.002

43. Geier N (2020) Influence of fibre orientation on cutting force in up and down milling of UD-CFRP composites. Int J Adv Manuf Technol 111:881–893. https://doi.org/10.1007/s00170-020-06163-3

44. Hosokawa A, Hirose N, Ueda T, Furumoto T (2014) High-quality machining of CFRP with high helix end mill. CIRP Ann Manuf Technol 63:89–92. https://doi.org/10.1016/j.cirp.2014.03.084

45. Kim G, Kim TG, Lee SW, Min BK (2022) Effect of workpiece preheating on tool wear and delamination at the hole exit in high feed drilling of carbon fiber reinforced plastics with diamond-coated tools. J Manuf Process 74:233–243. https://doi.org/10.1016/j.jmapro.2021.12.013

46. Wang H, Zhang D, Li Y, Cong W (2020) The effects of elliptical ultrasonic vibration in surface machining of CFRP composites using rotary ultrasonic machining. Int J Adv Manuf Technol 106:5527–5538. https://doi.org/10.1007/s00170-020-04976-w

47. Morkavuk S, Köklü U, Bağcı M, Gemi L (2018) Cryogenic machining of carbon fiber reinforced plastic (CFRP) composites and the effects of cryogenic treatment on tensile properties: a comparative study. Compos Part B 147:1–11. https://doi.org/10.1016/j.compositesb.2018.04.024

48. Kline WA, DeVor RE, Lindberg JR (1982) The prediction of cutting forces in end milling with application to cornering cuts. Int J Mach Tool Des Res 22:7–22. https://doi.org/10.1016/0020-7357(82)90016-6

49. Kline WA, DeVor RE (1983) The effect of runout on cutting geometry and forces in end milling. Int J Mach Tool Des Res 23:123–140. https://doi.org/10.1016/0020-7357(83)90012-4

50. Su Y (2019) Effect of the cutting speed on the cutting mechanism in machining CFRP. Compos Struct 220:662–676. https://doi.org/10.1016/j.compstruct.2019.04.052

51. Raschka S, Mirjalili V (2019) Python machine learning: machine learning & deep learning with python, Scikit-Learn and TensorFlow 2, Third edn. Packt Publishing, pp 195–197